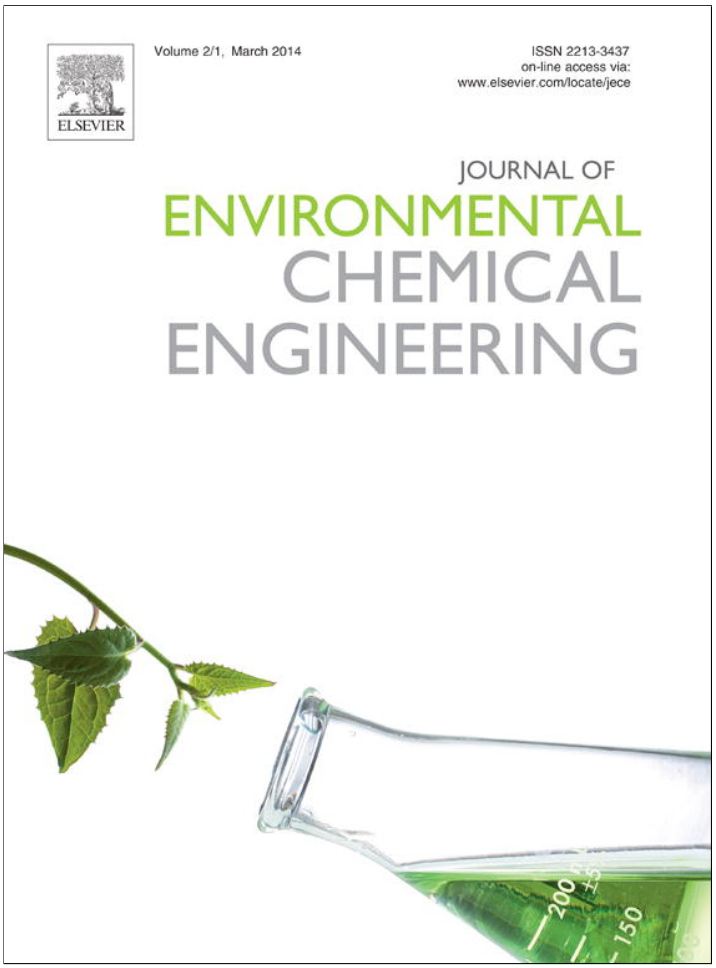

Journal of Environmental Chemical Engineering 2 (2014) 675–684

Contents lists available at ScienceDirect

Journal of Environmental Chemical Engineering

journal homepage: www.elsevier.com/locate/jece

Solid Phase Extraction of Hazardous metals from Aqua system by Nanoparticle-modified Agrowaste composite Adsorbents

Martins O. Omorogie [a,b,c], Jonathan O. Babalola [b,*], Emmanuel I. Unuabonah [c], Jian R. Gong [a,**]

[a] Laboratory for Nanodevices, National Center for Nanoscience and Technology (NCNST), 100190 Beijing, People's Republic of China
[b] Biophysical Chemistry Unit, Department of Chemistry, University of Ibadan, 200284, Ibadan, Nigeria
[c] Environmental and Chemical Processes Research Laboratory, Department of Chemical Sciences, Redeemer's University, P.M.B. 3005, Mowe 110115, Ogun State, Nigeria

ARTICLE INFO

Article history:
Received 15 June 2013
Received in revised form 6 November 2013
Accepted 7 November 2013

Keywords:
Nanoparticles
Agrowaste
Surface area
Kinetics
Adsorption
Thermodynamics

ABSTRACT

This study reports for the first time the adsorption of Cd(II) and Hg(II) ions from simulated wastewaters onto Nauclea diderrichii agrowaste (NDS) modified with mesoporous SiO_2 (MND) and mesoporous SiO_2 + graphene oxide (GND). Modification of NDS with mesoporous SiO_2 and graphene oxide improved its adsorption capacity for Cd(II) and Hg(II) in aqueous solution with surface area increasing from 5.4 m^2/g (in NDS) to 209 m^2/g (in MND) and 267 m^2/g (in GND) respectively. The modification of NDS also improved its rate of uptake of both metal ions with uptake rate of Hg(II) being more than that of Cd(II). Kinetic data obtained gave better fit to the pseudo-second order kinetic model than to pseudo-first order, Elovich, modified pseudo-first order, ion exchange or Weber–Morris intraparticle diffusion kinetic models. Data obtained from the Weber–Morris intraparticle diffusion model suggests that pore diffusion mechanism may have played a significant role in the adsorption process. Thermodynamic data showed negative and positive values for ΔG° and ΔH° respectively for the adsorption systems, which supports the fact that the adsorption of both Cd(II) and Hg(II) by MND and GND adsorbents was feasible, spontaneous and endothermic in nature.

Introduction

Global industrialization has led to an increase in the release of different pollutants into the ecosystems, many of which are non-biodegradable, thereby reducing the quality of the environment [1]. One of the most challenging issues in the globe today is that of environmental pollution caused by toxic heavy metals and their consequences on human life and ecology [1]. Contamination of various water bodies, land and biota by heavy metal ions has risen to levels that require urgent attention. Industrial activities are the major sources of cadmium {Cd(II)} and mercury {Hg(II)} ions including mining processes, metal plating, oil refining, electronic device manufacturing, printing, production of chemicals, dyes and paints, pulp and paper, textiles, petrochemicals, leather, fertilizers and pesticides [2,3].

Heavy metals are harmful to human health and to the environment due to their non-biodegradability. The World Health Organization (WHO) maximum tolerable limits for Cd(II) and Hg(II) ions in drinking water are 0.003 mg/L and 0.001 mg/L respectively [4]. They accumulate in living organisms causing various disorders. Hence, it is necessary to remove them from the ecosystem [5]. For instance, Cd(II) is one of the heavy metal ions found at the top of the toxicity list [5]. Due to its non-biodegradability, Cd(II) accumulates in plants and its level increases along the food chain. At higher trophic levels, the toxic effect of cadmium is more pronounced in animals. Cadmium toxicity has been reported as one of the causes of cancer, hypertension, weight loss, bone lesions and Itai–Itai disease [1,6,7].

Cadmium is transferred through the food chain system of soil–plant–animal–human into animals and human beings, causing severe health implications. Its accumulation in organs through the ingestion of cadmium-contaminated food leads to the malfunction of such organ, for example, spilling of protein into the urine from cadmium contaminated kidney which disrupts protein metabolism [7].

Mercury is generally considered the most toxic metal in ecosystems [8]. Its different toxic forms are mainly elemental mercury, inorganomercurials and organomercurials. Its toxicity depends on temperature, pH and the presence of chlorine and sulphur. [9]. In particular, methyl mercury has been shown to be extremely detrimental to childhood growth at very low doses [10] and causes impairment of the kidney, chest pain and dyspnea [11,12].

* Corresponding author. Tel.: +234 803 454 0881.
** Corresponding author. Tel.: +86 10 82545649.
E-mail addresses: bamijibabalola@yahoo.co.uk (J.O. Babalola), gongjr@nanoctr.cn (J.R. Gong).

2213-3437/$ – see front matter © 2013 Elsevier Ltd. All rights reserved.
http://dx.doi.org/10.1016/j.jece.2013.11.007

Various researchers have used different agrowastes to remove these toxic metals from industrial wastewaters because they are cheap and readily available [1–18]. Literature has shown lately that various adsorbents such as dried *Opuntia ficus indica* [19], *Spirodela polyrhiza* L. [20], goethite [21], resin grafted coconut activated charcoal [22], dithiocarbamate chelating resin [23], chitosan and chitosan derivatives [24], ionic liquids modified palm shell activated carbon [25], charcoal immobilized papain [26], bamboo leaf powder [27], triton-X and sodium dodecyl sulphate modified bamboo leaf powder [27], sodium-zeolite tuff [28], porous glass beads/chitosan support [29], *Nauclea diderrichii* [13,14], *Zea mays* seed chaff [30], defatted *Carica papaya* seed [31], *Carica papaya* seed-Kaolinite [2], etc. have been used for cadmium and mercury adsorption.

However, recent advances in materials science have also shown that various materials synthesized from various nanoparticles, especially magnetic nanoparticles which are easily regenerated, chitosan (due to its multi-functionalities), biomaterials, activated carbons and polymers, have been used for adsorption purpose. These materials have also played the role of solid supports for various biosorbents and as functionalization substances, in order to increase their adsorption capacities. Some of the materials that have been used for adsorption of Cd(II) and Hg(II) ions in current times are sawdust and neem bark [32], activated alumina [33], rice husk ash [34], modified sludge [35], 3-hydroxybenzaldehyde modified bentonite and activated bentonite [36], lignocellulosic waste material [37], polymer modified Fe_3O_4 magnetic nanoparticles [38], SiO_2 and Fe_3O_4 modified with chitosan and EDTA [39], alginate modified pectin gel beads [40], sulphur impregnated activated carbon [41], carbonaceous rice husk [42], thiol functionalized mesoporous silica [43], mercapto-functionalized nanomagnetic Fe_3O_4 polymer [44], poly(c-glutamic acid) biopolymer [45], ground-up tree fern [46], thiourea modified magnetic chitosan [47], diethylene triamine modified silica gel [48], polyamidoamine functionalized chitosan [49], polyacrylonitrile-N-chlorosulphonated polystyrene [50], amidoxime modified silica gel [51], polyamine modified silica [52], sulphur-amidoxime modified silica gel [53], Schiff's base modified magnetic chitosan resin [54] and mercapto-modified Fe_3O_4 magnetic nanosorbent [55]. However, the use of adsorbents of agricultural origin has a draw back known as 'bleeding' [2]. This is due to their biodegradability in aqueous media after some hours. Some adsorbents of agricultural origin also have the disadvantage that they do not possess the appropriate bulk densities needed for industrial applications [2].

Mesoporous materials have been applied in surface processes like catalysis and adsorption [56–59]. In recent times functionalities have been grafted to the surfaces of various types of mesoporous materials to selectively adsorb various pollutants of interest from aqueous media [60–62]. This study reports for the first time the adsorption capacities of a new class of adsorbent-nanoparticle modified agrowaste adsorbent, using *Nauclea diderrichii* agrowaste (NDS) modified with mesoporous SiO_2 and mesoporous SiO_2 + graphene oxide for the adsorption of Cd(II) and Hg(II) ions from simulated wastewater system.

As a follow up to our previous research work [13], this modification is aimed at improving the surface textural properties and functionalities of NDS and thus increasing its adsorption capacities and uptake rates for Cd(II) and Hg(II) ions.

Experimental

Preparation/characterizations of samples and adsorption study

Nauclea diderrichii agrowaste (NDS) was obtained from the Forest Research Institute of Nigeria (FRIN), in Ibadan (7°23′16″ North, 3°53′47″ East), Nigeria. After collection, it was heated in an oven at 60 °C for 3 h. Thereafter, it was pulverized and sieved to 450 μm particle size. Mesoporous SiO_2 was prepared by liquid templating method as described by Kresge et al. [56]. One gram of CTAB (Cethyl Trimethyl Ammonium Bromide) was weighed and dissolved in 480 mL deionized water. A 3.5 mL of 2 M NaOH was added to CTAB/H_2O solution. This was heated with an electric heater to 80 °C and the beaker containing the CTAB/H_2O solution was immersed in a silicone oil bath. The reaction mixture was agitated continuously at 1000 rpm for 1 h. Thereafter, 6 mL of TEOS (tetra ethyl ortho silicate) was added dropwisely to the reaction mixture and heated at 80 °C for 2 h. After cooling, the white precipitate formed was separated from the suspension using a separating funnel under vacuum. The white precipitate obtained was dried in an oven for 3 h at 100 °C before being calcined for 5 h at 550 °C [56].

The mesoporous SiO_2 prepared initially was subsequently added to NDS (in the ratio of 1:2, w/w) in 500 mL deionized water from Millipore water instrument. This reaction mixture was agitated at 1000 rpm at 20 °C for 48 h and the NDS + mesoporous SiO_2 (MND) was filtered via vacuum filtration. The wet MND was placed in an oven and dried at 100 °C overnight and kept for further use.

Graphene oxide was synthesized by chemical oxidation of natural graphite flake according to methods described by Hummers and Offeman [63]. Concentrated sulphuric acid and orthophosphoric acid (400:50 mL) were added to a mixture of $KMnO_4$ (30 g) and graphite (5 g). It was heated to 50 °C and stirred for 24 h. The resulting mixture was poured into ice (250 mL) and H_2O_2 (30%, 50 mL) and then filtered using a polycarbonate membrane. The solid product, graphene oxide was washed with water, 30% HCl, and ethanol two times before vacuum drying for 12 h using vacuum dessicator. The NDS + mesoporous SiO_2 + graphene oxide (GND) was also prepared by subsequently adding NDS, mesoporous SiO_2 and graphene oxide (in the ratio of 1:0.5:2, w/w) in 700 mL deionized water from Millipore water instrument. The reaction mixture was agitated at 1000 rpm at 20 °C for 48 h. The GND was also filtered by vacuum and wet GND was placed in a heating crucible and dried at 100 °C overnight. The GND was kept for further use. Thereafter, various surface characterizations of NDS, mesoporous SiO_2, graphene oxide, MND and GND were carried out using Perkin Elmer Spectrum 1 Fourier transform infra red (FTIR) spectrometer, Perkin Elmer Thermogravimetric analyzer (TG), X-ray diffractometer (XRD) D/Max-2500 (Rigaku, Japan) with Cu Kα radiation, λ = 0.154056 nm, Multipoint technique of nitrogen adsorption–desorption {Brunauer–Emmett–Teller (BET)} at 77 K by Micromeritics Instrument Corporation, ASAP 2020 Model analyzer, scanning electron microscope (SEM) (Hitachi S4800 Model) and transmission electron microscope (TEM), F20 S-TWIN, Tecnai G2, FEI Co.), at 200 kV accelerating voltage.

Adsorption experiments were carried out with fifty milligrams of MND and GND adsorbents were added to 20 mL of 20 mg/L Cd(II) and Hg(II) aqueous solutions, prepared from $Cd(NO_3)_2{\cdot}4H_2O$ and $Hg(NO_3)_2{\cdot}½H_2O$ of analytical grade, whose pH values were adjusted to 7.0 and 4.0 respectively (pH values of maximum adsorption were obtained from initial pH study {Data not shown}) with either 0.1 M HNO_3 or NaOH.

One thousand milligrams per liter of Cd(II) and Hg(II) aqueous solutions (simulated wastewater) were prepared by dissolving accurately weighed amounts of $Cd(NO_3)_2{\cdot}4H_2O$ and $Hg(NO_3)_2{\cdot}½H_2O$ (analytical grade) in 1 L of deionized water from Millipore water instrument. Furthermore, 20 mg/L of simulated wastewater containing Cd(II) and Hg(II) ions was prepared from 1000 mg/L by serial dilution.

For kinetic study, the suspensions under same conditions above were agitated in a rotary shaker. Samples were withdrawn at

various time intervals and filtered using filter papers. The supernatants obtained were analyzed for residual Cd(II) and Hg(II) ions using ICP-OES (Inductively Coupled Plasma-Optical Emission Spectrometer), Perkin Elmer Optima 5300DV Model. The amounts of Cd(II) and Hg(II) adsorbed by MND and GND were calculated by difference using the equation;

$$q_t = \frac{(C_0 - C_t)V}{W} \quad (1)$$

where C_0 is the initial concentration of metal ion (mg/L), C_t is the concentration of residual metal ion in the solution (mg/L) at time t (min), V is the volume of the aqueous solution containing metal ions (L), W is the weight of adsorbent (g) and q_t is the amount of metal ion adsorbed by the adsorbent (mg/g) at time t (min).

For thermodynamic study, a similar experiment as above was repeated at 303 K, 318 K and 333 K. Experimental data obtained were fitted to the Erying equation [64] which is expressed as;

$$\ln\left(\frac{k_2}{T}\right) = \ln\left(\frac{k}{h}\right) + \left(\frac{\Delta S^\circ}{R}\right) - \left(\frac{\Delta H^\circ}{RT}\right) \quad (2)$$

where k_2, k, h, R and T are pseudo-second order constant, Boltzmann constant, Planck constant, universal gas constant (J/mol K) and absolute temperature respectively.

Kinetic models

To understand how the time dynamics of these adsorption processes control the mechanism of the process such as the chemical reaction, mass transfer and diffusion control, the residence time of adsorbate was studied. Experimental data obtained were fitted to six kinetic models namely, pseudo-second order [65], pseudo-first order [66] Elovich [67], ion exchange [68], modified pseudo-first order [69], and Weber–Morris intraparticle diffusion [70] models. This is with the aim of finding the kinetic model that best describes the experimental data and hence the mechanism of the adsorption of the heavy metal ions the various adsorbents.

Pseudo-second order model

The linear form of the pseudo-second order model [65] is expressed as:

$$\frac{t}{q_t} = \frac{t}{q_e} + \frac{1}{k_2 {q_e}^2} \quad (3)$$

q_t is the amount of metal ion adsorbed at time t (min) by the biosorbent (mg/g) and k_2 is the pseudo-second order model rate constant (g/mg min). Also, the initial adsorption rate h (mg/g min), is written as:

$$h_{ads} = k_2 {q_e}^2 \quad (4)$$

Hence

$$\frac{t}{q_t} = \frac{t}{q_e} + \frac{1}{h_{ads}} \quad (5)$$

Pseudo-first order model

The linear form of the pseudo-first order model [66] is expressed as:

$$\ln(q_e - q_t) = \ln q_e - k_1 t \quad (6)$$

where q_t is the amount of metal ion adsorbed at time t (min) by the biosorbent (mg/g) and k_1 is the pseudo-second order model rate constant (/min).

Elovich kinetic model

The linear form of the Elovich equation [67] is expressed as:

$$q_t = \frac{1}{\beta}(\alpha\beta) + \frac{1}{\beta}\ln t \quad (7)$$

where α is the initial adsorption rate (mg/g min) and β (g/mg) is the Elovich constant related to the extent of surface coverage and the activation energy involved in chemisorption [71,72]. The Elovich kinetic equation describes adsorption processes that are chemisorptive in nature and it is suitable for systems with multilayer surfaces. In adsorption studies, Elovich kinetic model can also be used to predict the adsorption mechanism of the reactions taking place in the process [71,72].

Ion exchange kinetic model

This model considered the rates of ion exchange from aqueous solutions by zeolites (ion exchange resins) [68].

The linear form of the ion exchange kinetic model is expressed as:

$$\log(1 - F) = -\left(\frac{\nu}{2.303}\right)t \quad (8)$$

$F = q_t/q_e$, is the fractional attainment of equilibrium and ν (min^{-1}) is the ion exchange constant.

Modified pseudo-first order model

To solve the problem of multi-linearity that reduces the ability of the pseudo-first to well describe kinetic data [69], modified the pseudo-first order kinetic model was introduced and it is expressed as:

$$\frac{q_t}{q_e} + \ln(q_e - q_t) = \ln(q_e) - k_1' t \quad (9)$$

If the adsorption process follows the modified pseudo-first order kinetic model represented by Eq. (6), a plot of $q_t/q_e + \ln(q_e - q_t)$ against t gives a straight line.

Weber–Morris intraparticle diffusion model

Sorption process can be described by some consecutive steps starting with liquid film diffusion, internal diffusion and sorption of the solute on the interior surfaces of the pores and capillaries space of adsorbent. The Morris–Weber intraparticle diffusion model is expressed as:

$$q_t = K_{id} t^{1/2} + \psi \quad (10)$$

where K_{id} represents the Weber–Morris intraparticle diffusion constant (mg/g min$^{1/2}$) and ψ is a constant that gives information about the thickness of the boundary layer [70].

Homogeneous particle diffusion (HPD) model

In the homogenous model, the medium is seen as homogeneous and gel like. The solute is adsorbed at the particle surface and diffuses toward the center in a process governed by a driving force due to gradient in the adsorbed solute concentration, and a diffusion coefficient [73]. The rate determining step in this model is usually described by either;

(a) diffusion of ions through the liquid film surrounding the particle, called the film diffusion;
(b) diffusion of ions into sorbent beads called particle diffusion mechanism [74]. Diffusion rate constant is given as follow;

$$X(t) = 1 - \frac{6}{\pi^2}\sum_{Z=1}^{\infty}\frac{1}{Z^2}\exp\left[\frac{-Z^2\pi^2 D_e t}{r^2}\right] \quad \text{(Fickian equation)} \quad (11)$$

Fickian equation was approximated to Vermeulen equation [75] in Eq. (12) below to fit a range $0 < X(t) < 1$. For adsorption on

spherical particles.

$$X(t) = \left[1 - \exp\left[\frac{-Z^2\pi^2 D_e t}{r^2}\right]\right]^{1/2} \quad \text{(Vermeulen equation)} \qquad (12)$$

The above equation can be expressed as

$$-ln\,(1 - X^2(t)) = 2Kt$$

where $K = \pi^2 D_e/r^2$

If liquid film diffusion controls the rate of adsorption, the following analogous expression can be used:

$$X(t) = 1 - \exp\left[\frac{-3D_e C_t}{r\delta C_r}\right] \qquad (13)$$

$$-\ln\,(1 - X(t)) = K_{Li}t \qquad (14)$$

where $K_{Li} = 3D_eC/r\delta C_r$is the fractional attainment of equilibrium at time $t = q_t/q_e$, D_e is the effective diffusion coefficient of sorbates in the sorbent phase ($m^2\,s^{-1}$), r is the radius of the adsorbent particle assumed to be spherical (m), Z is the integer, C is the total concentration of both exchanging species (mg/L), C_r is the total concentration of both exchanging species in the ion exchanger (mg/L), K_{Li} is the rate constant for film diffusion (infinite solution volume condition) ($m\,s^{-1}$), δ is the thickness of liquid film

Eq. (14) can also be given below as:

$$-\ln\left[1 - \frac{q_t}{q_e}\right] = \frac{3D_eC}{r\delta C_r}t \qquad (15)$$

Hence, the effective diffusion coefficients, D_e of the liquid film diffusion process are calculated from the slopes of the plots of $-\ln[1 - (q_t/q_e)]$ against t, with zero intercept.

Results and discussion

Surface microstructural characterization techniques

Fourier transform infra red (FTIR) spectroscopy

Fig. 1(a) and (b) shows the FTIR spectra of NDS, mesoporous SiO_2, MND, GND and graphene oxide respectively. The FTIR spectrum of NDS was described by Omorogie et al. [14].

The FTIR spectrum of mesoporous SiO_2 showed a broad peak at 3400 cm^{-1} which is assigned to the –OH of silanol [76]. The peak at 2900 cm^{-1} is assigned to –C–H of $–CH_2$ and $–CH_3$ of aliphatic chains of the cationic surfactant (CTAB) and the Si precursor [76]. The peak at 1730 cm^{-1} is assigned to R–NH_3^+ group in the cationic surfactant. The 1210 cm^{-1} and 920 cm^{-1} bands are the –Si–O– and –Si–O–Si– bending vibrations respectively which are from the silica framework [76]. In the MND spectrum, the broad peak at 3400 cm^{-1} found in the mesoporous SiO_2 disappeared, probably due to the formation of hydroxylated complexes during the preparation of the solid phase extractant. An observed peak at 1700 cm^{-1} is assigned to –C=O stretch of carboxylate group [76]. The –Si–O– vibration band observed in mesoporous SiO_2 shifted significantly from 1210 to 1100 cm^{-1} with the disappearance of the 920 cm^{-1} suggesting the possibility of mesoporous SiO_2 interacting with the –OH groups in NDS. The graphene oxide gave vibrational signals at 3500 cm^{-1} for OH stretch, 1760–1720 cm^{-1} for C=O stretches of ketones and aldehydes, 1240–1230 cm^{-1} for C–O stretch and 1050 cm^{-1} for C–O bend [77]. The GND gave vibrations at 3500 cm^{-1} for OH stretch, 2900 cm^{-1} for asymmetric C–H stretches of methylene and methyl groups, 1450 cm^{-1} for C=C stretch, 1205 cm^{-1} for C–C and C–O stretches, 805 cm^{-1} for C–C and C–H out of plane bends [17].

Thermogravimetric (TG) analysis

Fig. 2 shows the TG thermograms of graphene oxide, mesoporous silica, NDS, GND and MND. The TG thermogram of NDS has been previously described by Omorogie et al. [14]. The TG thermogram for mesoporous SiO_2 was observed to show a weight loss between 80 and 1000 °C (ca. 6%), which is possibly due to loss of water molecules and the cationic surfactant used in synthesizing it [76]. However, MND showed initial weight loss of ca. 9% due to loss in water from 50 to 100 °C and ca. 50% (from 250 to 600 °C) due to loss of organics such as the cationic surfactant and some carbonaceous materials which are constituents of MND [19]. The graphene oxide indicated weight losses of ca. 11% from 20 to 200 °C, ca. 70% from 250 to 900 °C due to loss of surface water, solvent and carbon based precursor decomposition respectively [77]. Then GND indicated weight losses of ca. 10% from 20 to 250 °C and ca. 40% from 250 to 650 °C owing to loss of surface water and cationic surfactant and decomposition of volatile matter with some decomposition of cellulosics/lignin.

Scanning electron microscopy (SEM), transmission electron microscopy (TEM) and Brunauer–Emmett–Teller (BET) nitrogen adsorption–desorption at 77 K

Fig. 3(a) and (b) shows the SEM images of mesoporous SiO_2, Fig. 3(c) shows the TEM image of mesoporous SiO_2 and Fig. 3(d) shows the SEM image of graphene oxide. The SEM image of NDS

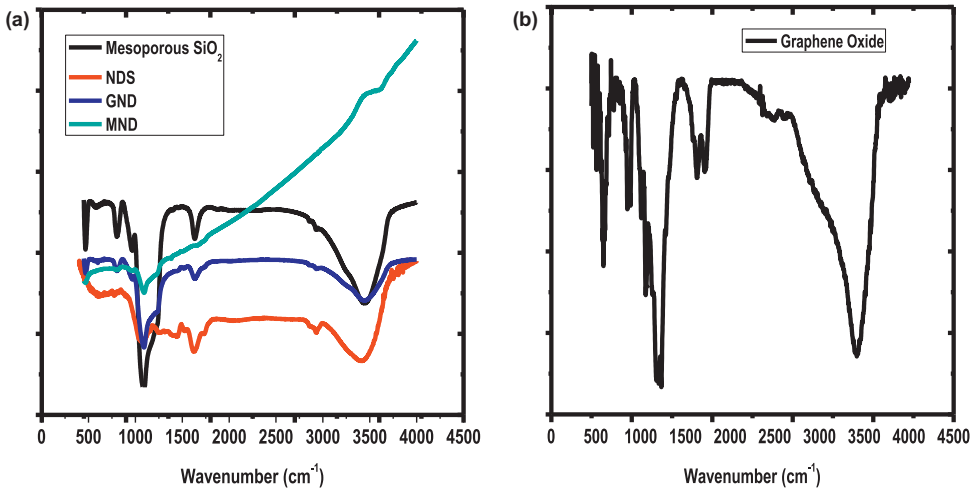

Fig. 1. FTIR spectra of (a) mesoporous SiO_2, NDS, GND and MND (b) graphene oxide.

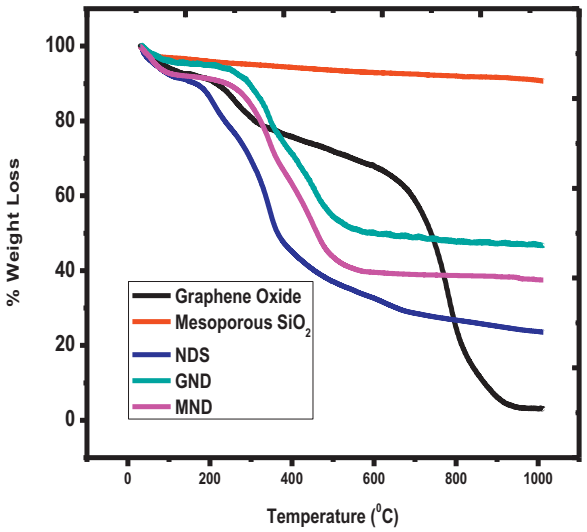

Fig. 2. Thermogravimetric analytical profiles for graphene oxide, mesoporous silica, NDS, GND and MND.

was described by Omorogie et al. [13,14]. The SEM images of mesoporous SiO_2 revealed monodispersed array of mesopores with uniform particles on the surface. The TEM image of mesoporous SiO_2 showed nanoparticles at 50 nm, which is typical of mesoporous materials with particle diameter of 2–50 nm [56]. The SEM image of graphene oxide revealed particles in the macropore range with cross sectional pores on the surface, while those of MND and GND (not shown) indicated large particles due to the presence of NDS. Nitrogen absorption–desorption analysis showed that the BET surface areas at 77 K of NDS increased from 5.4 m^2/g to 209 m^2/g and 267 m^2/g in MND and GND respectively. This increase is due to the introduction mesoporous SiO_2 (specific surface area = 1098.3 m^2/g) and graphene oxide (specific surface area = 33.7 m^2/g) into NDS. The BET adsorption average pore width for NDS, MND and GND adsorbents are 3.014 nm, 4.631 nm and 4.365 nm respectively which suggests that modification of NDS agrowaste increased both its pore width and pore volume. The improved pore width and pore volume of MND and GND adsorbents with respect to those of NDS agrowaste were in part, responsible for the increase in the uptake of Cd(II) and Hg(II) ions onto them. Fig. 4(a) and (b) shows the BET nitrogen isotherm plots of MND and GND respectively.

Adsorption kinetics and thermodynamics

Experimental data obtained from kinetic studies were fitted to six kinetic models namely, pseudo-second order, pseudo-first order, Elovich, ion exchange, modified pseudo-first order, and Weber–Morris intraparticle diffusion models.

The pseudo-first order and modified pseudo-first order kinetic models gave correlation co-efficients, $R^2 < 0.97$ and rate constants, $k_1 \leq 0.041\ min^{-1}$ and $k_1 \leq 0.0450\ min^{-1}$ respectively for all cases. Elovich, Morris–Weber and ion exchange kinetic models gave correlation co-efficients, $R^2 \leq 0.9807$ for all cases.

The pseudo-second order kinetic model gave best fit to the experimental data with rate constant $k_2 \leq 0.872$ g/mg min and correlation coefficients values, $R^2 \leq 1$ for all cases. The initial sorption rates h, for the uptake of Cd(II) and Hg(II) by MND are ≤8.3455 mg/g min and ≤40.7959 mg/g min respectively. Also, the initial sorption rates h, for the uptake of Cd(II) and Hg(II) by GND are ≤7.6029 mg/g min and ≤16.6205 mg/g min respectively. From the Pseudo-second order kinetic model, the adsorption capacity (q_e) was observed to increase with increasing temperature with capacity being higher for Cd(II) ions than for Hg(II) ions for both adsorbents (Table 1). The kinetic q_e values obtained experimental

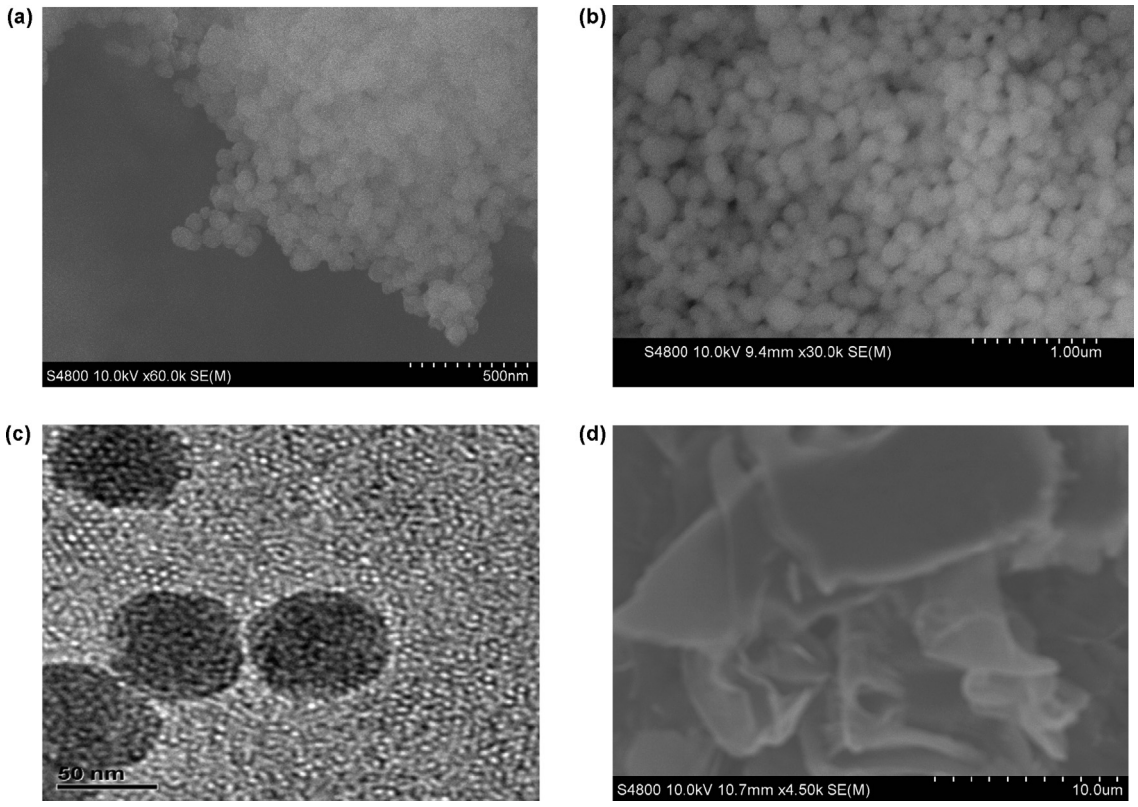

Fig. 3. (a, b) SEM images of mesoporous SiO_2, (c) TEM image of mesoporous SiO_2, (d) SEM image of graphene oxide.

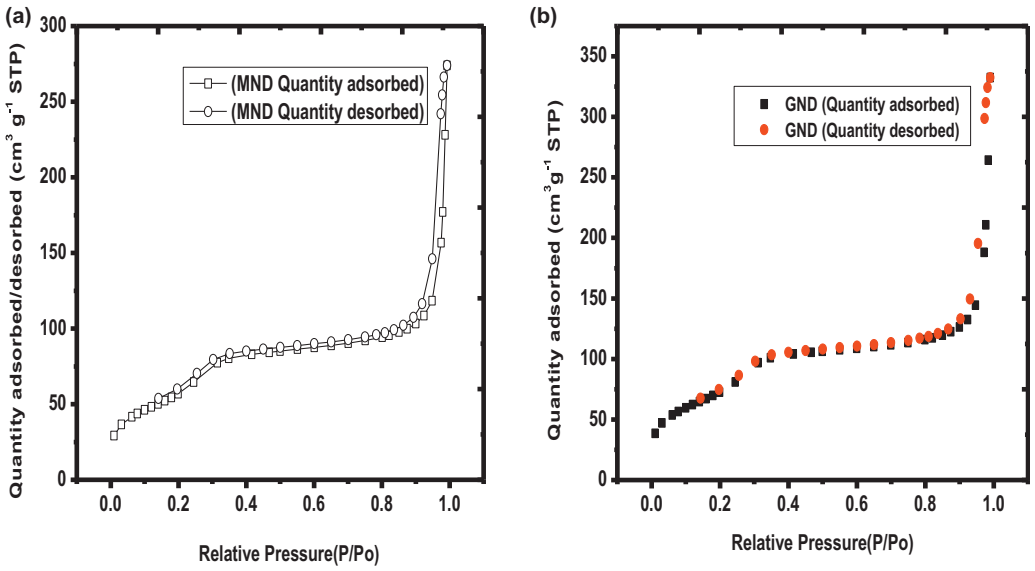

Fig. 4. BET nitrogen adsorption–desorption isotherm plots of (a) MND and (b) GND.

Table 1
Kinetic parameters for the adsorption of Cd(II) and Hg(II) ions by MND and GND.

	MND						GND					
	Cd(II)			Hg(II)			Cd(II)			Hg(II)		
	303 K	318 K	333 K	303 K	318 K	333 K	303 K	318 K	333 K	303 K	318 K	333 K
Pseudo-1st order												
R^2	0.5593	0.8867	0.8610	0.9649	0.8877	0.6858	0.7378	0.7517	0.8482	0.8091	0.8781	0.8071
q_e (mg/g)	1.1274	2.5216	1.7812	0.2780	0.3342	0.2663	1.5736	1.5876	1.5529	1.3051	0.7095	1.2029
k_1 (/min)	0.0269	0.0298	0.0336	0.0410	0.0359	0.0356	0.0299	0.0172	0.0347	0.0243	0.0352	0.0255
$q_{e(exp)}$ (mg/g)	6.8500	7.1200	7.4800	6.8200	6.8300	6.5600	7.1200	7.1400	7.5100	7.2900	6.8800	7.1800
Modified pseudo-1st order												
R^2	0.5986	0.9144	0.9054	0.9655	0.8918	0.6877	0.8263	0.8244	0.7770	0.7815	0.7641	0.8248
q_e (mg/g)	2.5493	4.8954	3.7743	0.7312	0.8663	0.6910	1.9970	2.7590	3.4009	3.4431	3.7540	2.9678
k_1' (min)	0.0236	0.0262	0.0308	0.0406	0.0354	0.0351	0.0450	0.0228	0.0259	0.0144	0.0403	0.0216
$q_{e(exp)}$ (mg/g)	6.8500	7.1200	7.4800	6.8200	6.8300	6.5600	7.1200	7.1400	7.5100	7.2900	6.8800	7.1800
Pseudo-2nd order												
R^2	0.9992	0.9983	0.9997	1.0000	1.0000	1.0000	0.9991	0.9963	0.9998	0.9990	1.0000	0.9992
q_e (mg/g)	6.8292	7.2359	7.5245	6.5660	6.8297	6.8399	7.0867	7.1220	7.5409	6.8908	7.1073	7.2754
K_2 (g/mg min)	0.0577	0.1084	0.1474	0.6497	0.7796	0.8720	0.0727	0.1070	0.1337	0.1098	0.1271	0.3140
$q_{e(exp)}$ (mg/g)	6.8500	7.1200	7.4800	6.8200	6.8300	6.5600	7.1200	7.1400	7.5100	7.2900	6.8800	7.1800
Elovich												
R^2	0.8586	0.9205	0.8900	0.9119	0.9743	0.8992	0.9488	0.9333	0.9193	0.9380	0.9325	0.9807
α (mg/g min)	4.679	274.6275	682.3203	1.6090	3.4490	2.0590	5.0000	1.7200	23.3300	1.2000	3.7800	1.4100
β (g/mg)	2.6991	1.4986	1.4661	15.3139	9.5694	10.6157	2.2813	2.9705	1.6363	3.4485	4.0182	3.5295
$q_{e(exp)}$ (mg/g)	6.8500	7.1200	7.4800	6.8200	6.8300	6.5600	7.1200	7.1400	7.5100	7.2900	6.8800	7.1800
Ion exchange												
R^2	0.5593	0.8867	0.8610	0.9649	0.8877	0.6858	0.7378	0.7517	0.8482	0.8091	0.8781	0.8071
υ (min)	0.0269	0.0298	0.0336	0.0409	0.0359	0.0356	0.0299	0.0172	0.0348	0.0242	0.0352	0.0256
$q_{e(exp)}$ (mg/g)	6.8500	7.1200	7.4800	6.8200	6.8300	6.5600	7.1200	7.1400	7.5100	7.2900	6.8800	7.1800
Morris–Weber												
R^2	0.5667	0.8155	0.5719	0.7286	0.7499	0.7616	0.7202	0.9129	0.6002	0.8778	0.6787	0.8790
k_{id} (g/mg min$^{1/2}$)	0.1699	0.3463	0.3092	0.0324	0.0509	0.0479	0.2128	0.1824	0.2787	0.1541	0.1187	0.1477
Ψ	5.3187	4.0571	4.9364	6.5342	6.4004	6.1564	5.1911	5.1885	5.2351	5.7563	5.8920	5.6889
$q_{e(exp)}$ (mg/g)	6.8500	7.1200	7.4800	6.8200	6.8300	6.5600	7.1200	7.1400	7.5100	7.2900	6.8800	7.1800
Homogeneous particle diffusion												
R^2	0.5840	0.7972	0.7564	0.8836	0.7164	0.8994	0.6504	0.5510	0.7425	0.8451	0.4891	0.5966
K_{Li} (m/s)	0.0760	0.0439	0.0529	0.0618	0.1443	0.0414	0.0731	0.0570	0.0559	0.1334	0.0422	0.0411
D_e[a] $\times 10^{-9}$	1.5589	0.9005	1.0851	1.2677	2.9599	0.8492	1.4994	1.1692	1.1466	2.7363	0.8656	0.8431
$q_{e(exp)}$ (mg/g)	6.8500	7.1200	7.4800	6.8200	6.8300	6.5600	7.1200	7.1400	7.5100	7.2900	6.8800	7.1800

[a] D_e (m/s).

are not significantly different from those obtained from equilibrium isotherms [78].

From this data, it is interesting to note that the initial sorption rates for the uptake of Hg(II) by MND and GND were higher than those of Cd(II) even though the adsorption capacities of MND and GND for Cd(II) are slightly greater than those of Hg(II). Of interest, is the fact that the highest initial sorption rate of NDS for Cd(II) was 56.1855 mg/g min [13], which is far greater than those of MND and GND. But, MND and GND show better initial sorption rates for Hg(II) than NDS [13]. No possible explanation can be offered for this now. However we believe that the change in surface properties from NDS to MND and GND could have influenced this trend. From the Weber–Morris intraparticle diffusion model, adsorption of Cd(II) and Hg (II) onto MND and GND seem to be more controlled by film diffusion (external mass transport) than intraparticle diffusion while the reverse is the case with NDS [13]. The initial sorption rates obtained from kinetic data showed that modification of NDS with mesoporous SiO_2 and graphene oxide are more significant for the removal of Hg(II) from aqueous solution than Cd(II).

The intercept values from the Weber–Morris intraparticle diffusion model, ψ, which represents the thickness of the boundary layer obtained from experimental data for the adsorption of Cd(II) and Hg(II) by MND and GND were > 0 (see Table 1). This indicates that both film and pore diffusions were involved in the rate-controlling step of the adsorption processes [65].

Experimental data showed that modifying NDS with mesoporous SiO_2 and graphene oxide slightly increased its adsorption capacities for Cd(II) and Hg(II) [13]. However, Cd(II) ion was adsorbed slightly more than Hg(II) ion by MND and GND when compared to NDS even though they have similar ionic radii (Cd(II) ion, 0.097 nm and Hg(II) ion, 0.100 nm) [18]. However, the hydration energy of Cd(II) (1807 kJ/mol) is lower than that of Hg(II) (1824 kJ/mol), which suggests that Cd(II) loses its hydration shell easily and is thus more adsorbed than Hg(II) [2,79,80].

From Elovich kinetic model, the initial adsorption rates α, for the uptake of Cd(II) and Hg(II) ions onto MND and GND adsorbents were between 1.2 and 682.32 mg/g min, with that of Cd(II) ion onto MND being the highest. This simply implies that the initial adsorption rates of uptake of Cd(II) ion were higher than those of Hg(II) ion onto MND and GND. Hence, this might be responsible for the slight increase in the adsorption capacities of MND and GND adsorbents for Cd(II) ion over those of Hg(II) ion.

Also, β, which is the Elovich constant is related to the extent of surface coverage of adsorbents by adsorbates and the energy involved in chemisorption gave an indication that the uptake of Cd(II) and Hg(II) ions onto MND and GND adsorbents were between 1.5 and 15.31 g/mg. These values show that the mode of adsorption of Cd(II) and Hg(II) ions onto MND and GND adsorbents was chemisorptive in nature [71,72].

The homogeneous particle diffusion (HPD) model gave the effective diffusion coefficients of sorbates in the sorbent phase, D_e, in the range of $0.8431–2.9599 \times 10^{-9}$ m^2/s. Also, the rate constants for film diffusion, K_{Li}, were 0.0411–0.1443 m/s. It is interesting to note that mesoporous SiO_2 + graphene oxide modified NDS (GND) in this study performed better than mesoporous SiO_2 modified NDS (MND) and NDS for the uptake of Cd(II) and Hg(II) ions in simulated wastewater. The reason for this is associated with the fact that graphene oxide has π–π stacking interaction which plays a significant role in adsorption [80]. Also, graphene oxide comprises a variety of oxygen-based chemical functional groups on its basal planes and edges. These oxygen-based functional moieties, such as epoxide, hydroxyl, and carboxylic groups account for the adsorption affinity of graphene oxide for basic and cationic compounds [81,82]. Another reason is that mesoporous SiO_2 has excellent surface area (from N_2

Table 2
Thermodynamic parameters for the adsorption of Cd(II) and Hg(II) ions by MND and GND.

	MND						GND					
	Cd(II)			Hg(II)			Cd(II)			Hg(II)		
	303 K	318 K	333 K	303 K	318 K	333 K	303 K	318 K	333 K	303 K	318 K	333 K
$-\Delta G^\circ$ (kJ/mol)	19.837	21.409	22.981	15.152	16.084	17.015	20.425	21.280	22.136	19.179	20.014	20.849
$+\Delta H^\circ$ (kJ/mol)	11.915			3.663			3.148			2.308		
$+\Delta S^\circ$ (J/mol K)	104.793			62.096			57.020			55.679		

adsorption–desorption analysis) and functional groups (Si–O– and –Si–O–Si–). In the overall, the modification of NDS with mesoporous SiO_2 + graphene oxide and mesoporous SiO_2 increased the chemical functionalities and surface area of NDS which improved the adsorption capacity of GND and MND adsorbents for Cd(II) and Hg(II) ions over NDS. Also, TG analysis has shown that GND and MND adsorbents will overcome the challenge of thermo-degradation and bleeding [2] that is generally associated with biosorbents. Another implication of this modification is that it improves the ability of NDS adsorbent in the adsorption of adsorbates from aqueous solution at high temperatures.

Temperature is very important in adsorption processes. Like other chemical reactions, some adsorption processes are kinetically driven by temperature. It predicts to a great extent the mass transfer of adsorbates (metal ions) from the bulk solution phase to the active sites on the adsorbents, and also account for diffusion processes during adsorption [65]. Calculations for the thermodynamic parameters from experimental data of the adsorption of Cd(II) and Hg(II) by MND and GND adsorbents indicate that ΔG° and ΔH° values were all negative and positive respectively for the adsorption process. Table 2 shows that adsorption of both Cd(II) and Hg(II) by MND and GND adsorbents was feasible and spontaneous with increasing temperature, as this is supported by the endothermic nature of the reaction. The positive ΔS° values for the adsorption process of both metal ions indicate an increase in the degree of chaos for their uptake onto both adsorbents, prompted by strong interactions between the metal ions and the surface of the adsorbents. The spontaneity of the adsorption reaction is confirmed from the negative ΔG° values (Table 2) with the adsorption of Hg(II) being more spontaneous than that of Cd(II) for both adsorbents. The increase in ΔG° values for the adsorption of Cd(II) by NDS, MND and GND adsorbents over those of Hg(II) perhaps shows that a stronger bond is formed with its surface resulting in a complex. Fig. 5(a) and (b) shows the non linear plots of q_t (mg/g) of Cd(II) and Hg(II) ions adsorbed by MND and GND against time t (min) at 303 K, 318 K and 333 K respectively.

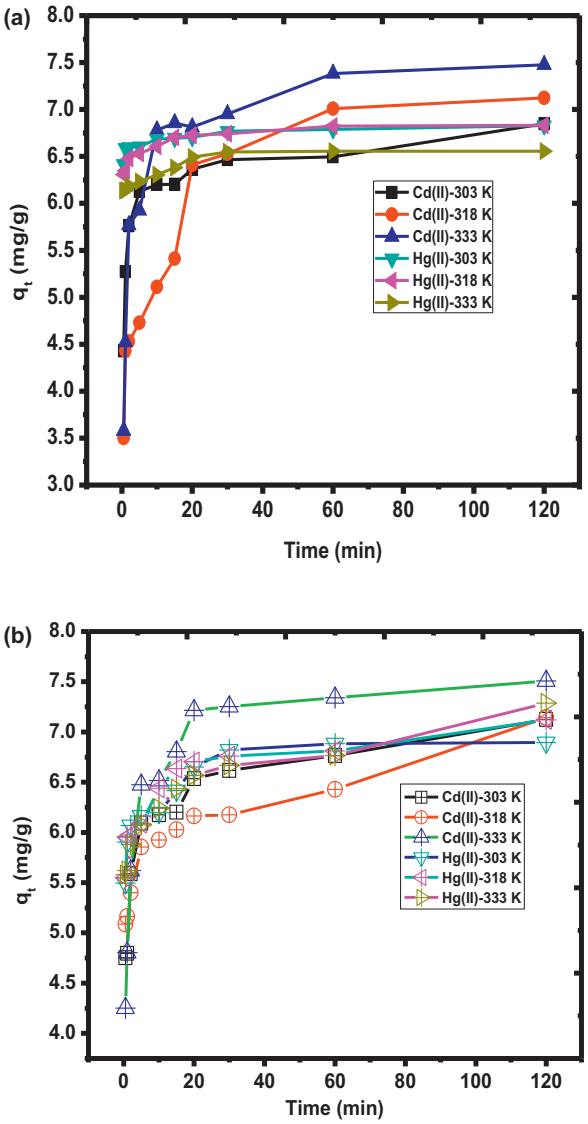

Fig. 5. (a) Non linear plots of q_t (mg/g) of Cd(II) and Hg(II) adsorbed by MND against time t (min) at temperatures of 303 K, 318 K and 333 K respectively. (b) Non linear plots of q_t (mg/g) of Cd(II) and Hg(II) ions adsorbed by GND against time t (min) at temperatures of 303 K, 318 K and 333 K respectively.

Conclusion

The findings from this work has revealed that the sequestration of Cd(II) and Hg(II) ions from simulated wastewater system by two new class of adsorbents, *Nauclea diderrichii* agrowaste (NDS) modified with mesoporous SiO_2 (MND) and mesoporous SiO_2 + - graphene oxide (GND) gave very good adsorption performance for Cd(II) and Hg(II) in aqueous. This is due to the improved surface properties of NDS after the modification. Experimental data best fit the pseudo-second order kinetic model compared with others. Studies with the experimental data using Weber–Morris intra-particle diffusion model indicated that pore diffusion mechanism might have played a more significant role in the adsorption of the metal ions onto MND and GND adsorbents than NDS agrowaste material. The rates of uptake of Hg(II) kinetically in aqueous media on the MND and GND adsorbents are higher than those for Cd(II). Both adsorbents exhibited good adsorption capacities for the removal of these recalcitrant metal ions (Hg(II) and Cd(II)) from simulated wastewater systems than NDS agrowaste material [12].

Acknowledgements

The authors acknowledge the support of The World Academy of Sciences-for the advancement of science in developing countries (TWAS), Italy and the Chinese Academy of Sciences (CAS), China for providing Fellowship (FR Number: 3240240234) to Martins O. Omorogie at the Laboratory for Nanodevices of the National Center for Nanoscience and Technology, Beijing, China where this research was done. This work was also supported in part by the National Basic Research Program of China (973 Program No. 2011CB933401) and the National Natural Science Foundation of China (21005023). Prof. Jian R. Gong gratefully acknowledges the support of the K.C. Wong Education Foundation, Hong Kong.

References

[1] Y.C. Sharma, Thermodynamics of removal of cadmium by adsorption on an indigenous clay, Chem. Eng. J. 145 (2008) 64–68.
[2] E.I. Unuabonah, C. Gunter, J. Weber, S. Lubahn, A. Taubert, Hybrid clay: a new highly efficient adsorbent for water treatment, ACS Sust. Chem. Eng. 1 (8) (2013) 966–973.
[3] V.C. Srivastava, I.D. Mall, I.M. Mishra, Competitive adsorption of cadmium(II) and nickel(II) metal ions from aqueous solution onto rice husk ash, Chem. Eng. Process. 48 (2009) 370–379.
[4] World Health Organisation, Guidelines for Drinking Water Quality. Recommendations, WHO, Geneva, 1984.
[5] K.S. Low, C.K. Lee, S.C. Liew, Sorption of cadmium and lead from aqueous solutions by spent grain, Process Biochem. 36 (2000) 59–64.
[6] S.E. Manahan, Environmental Chemistry, 6th ed., Lewis Publishers, Boca Raton, 1994.

[7] M.B. Kirkham, Cadmium in plants on polluted soils: effects of soil factors, hyperaccumulation and amendments, Geoderma 137 (2006) 19–32.
[8] T.W. Clarkson, Mercury major issues in environmental health, Environ. Health Perspect. 100 (1993) 31–38.
[9] S.H. Lee, Y.J. Rhym, S.P. Cho, J.I. Baek, Carbon-based novel sorbent for removing gas-phase mercury, Fuel 85 (2006) 219–226.
[10] F. Dobes, E. Budtz-Jorgensen, P. Weihe, R.F. White, P. Grandjean, Impact of prenatal methylmercury exposure on neurobehavioral function at age 14 years, Neurotoxicol. Teratol. 28 (2006) 536–547.
[11] F. Berglund, M. Bertin, Chemical Fallout, Thomas Publishers, Springfield, 1969.
[12] C.R. Krishnamoorthi, P. Vishwanathan, Toxic Metal in Indian Environment, Tata McGraw Hill, New Delhi, 1991.
[13] M.O. Omorogie, J.O. Babalola, E.I. Unuabonah, J.R. Gong, Kinetics and thermodynamics of heavy metal ions sequestration onto novel *Nauclea diderrichii* seed biomass, Bioresour. Technol. 118 (2012) 576–579.
[14] M.O. Omorogie, J.O. Babalola, E.I. Unuabonah, W. Song, J.R. Gong, Efficient chromium abstraction from aqueous solution using a low-cost biosorbent: *Nauclea diderrichii* seed waste, J. Saudi Chem. Soc. (2012), http://dx.doi.org/10.1016/j.jscs.2012.09.017 (in press).
[15] S.-Y. Kang, J.U. Lee, K.-W. Kim, Biosorption of Pb(II) from synthetic wastewater onto *Pseudomonas aeruginosa*, J. Environ. Pollut. V34 (1–4) (2008) 195–202.
[16] S. Gupta, B.V. Babu, Utilization of waste product (Tamarind seeds) for the removal of Cr(VI) from wastewater: equilibrium, kinetics and regeneration studies, J. Environ. Manage. 90 (2009) 3013–3022.
[17] S.H. Hasan, P. Srivastava, M. Talat, Biosorption of Pb(II) from water using biomass of *Aeromonas hydrophila*: central composite design for optimization of process variables, J. Hazard. Mater. 168 (2009) 1155–1162.
[18] R. Yan, F. Yang, Y. Wu, Z. Hu, B. Nath, L. Yang, Y. Fang, Cadmium and mercury removal from non-point source wastewater by a hybrid bioreactor, Bioresour. Technol. 102 (2011) 9927–9932.
[19] N. Barka, M. Abdennouri, M. El Makhfouk, S. Qourzal, Biosorption characteristics of cadmium and lead onto eco-friendly dried cactus (*Opuntia ficus indica*) cladodes, J. Environ. Chem. Eng. (2013), http://dx.doi.org/10.1016/j.jece.2013.04.008 (in press).
[20] M.D. Meitei, M.N.V. Prasad, Lead(II) and cadmium(II) biosorption on *Spirodela polyrhiza* (L.) Schleiden biomass, J. Environ. Chem. Eng. (2013), http://dx.doi.org/10.1016/j.jece.2013.04.016 (in press).
[21] A. Jaiswal, S. Banerjee, R. Mani, M.C. Chattopadhyaya, Synthesis, characterization and application of goethite mineral as an adsorbent, J. Environ. Chem. Eng. (2013), http://dx.doi.org/10.1016/j.jece.2013.05.007 (in press).
[22] G.-P. Jin, X.-H. Zhu, C.-Y. Li, Y. Fu, J.-X. Guan, X.-P. Wua, Tetraoxalyl ethylenediamine melamine resin functionalized coconut active charcoal for adsorptive removal of Ni(II), Pb(II) and Cd(II) from their aqueous solution, J. Environ. Chem. Eng. (2013), http://dx.doi.org/10.1016/j.jece.2013.07.010 (in press).
[23] A.F. Shaaban, D.A. Fadel, A.A. Mahmoud, M.A. Elkomy, S.M. Elbahy, Synthesis and characterization of dithiocarbamate chelating resin and its adsorption performance toward Hg(II), Cd(II) and Pb(II) by batch and fixed-bed column methods, J. Environ. Chem. Eng. (2013), http://dx.doi.org/10.1016/j.jece.2013.04.014 (in press).
[24] P. Miretzkya, A.F. Cirelli, Hg (II) removal from water by chitosan and chitosan derivatives: a review, J. Hazard. Mater. 167 (2009) 10–23.
[25] A.A. Ismaiel, M.K. Aroua, R. Yusoff, Palm shell activated carbon impregnated with task specific ionic-liquids as a novel adsorbent for the removal of mercury from contaminated water, Chem. Eng. J. 225 (2013) 306–314.
[26] S. Dutta, A. Bhattacharyya, P. De, P. Ray, S. Basu, Removal of mercury from its aqueous solution using charcoal-immobilized papain (CIP), J. Hazard. Mater. 172 (2009) 888–896.
[27] D. Kumar, M. Barun, K. Nandi, M.K. Purkait, Removal of mercury (II) from aqueous solution using bamboo leaf powder: equilibrium, thermodynamic and kinetic studies, J. Environ. Chem. Eng. (2013), http://dx.doi.org/10.1016/j.jece.2013.07.034 (in press).
[28] E. Gutiérrez-Segura, M. Solache-Ríos, A. Colín-Cruz, C. Fall, Adsorption of cadmium by Na and Fe modified zeolitic tuffs and carbonaceous material from pyrolyzed sewage sludge, J. Environ. Manage. 97 (2012) 6–13.
[29] C. Shen, Y. Wang, J. Xu, G. Luo, Chitosan supported on porous glass beads as a new green adsorbent for heavy metal recovery, Chem. Eng. J. 229 (2013) 217–224.
[30] J.O. Babalola, M.O. Omorogie, A.A. Babarinde, E.I. Unuabonah, V.O. Oninla, Optimization of the biosorption of Cr^{3+}, Cd^{2+} and Pb^{2+} using a new biowaste: *Zea mays* Seed Chaff, Environ. Eng. Manage. J. (2013) (in press) http://omicron.ch.tuiasi.ro/EEMJ/accepted.htm.
[31] U.G. Adie, E.I. Unuabonah, A.A. Adeyemo, G.O. Adeyemi, Biosorptive removal of Pb^{2+} and Cd^{2+} onto novel biosorbent: defatted *Carica papaya* seeds, Biomass Bioenergy 35 (2011) 2517–2525.
[32] T.K. Naiya, P. Chowdhury, A.K. Bhattacharya, S.K. Das, Saw dust and neem bark as low-cost natural biosorbent for adsorptive removal of Zn (II) and Cd (II) ions from aqueous solutions, Chem. Eng. J. 148 (2009) 68–79.
[33] T.K. Naiya, A.K. Bhattacharya, S.K. Das, Adsorption of Cd (II) and Pb (II) from aqueous solutions on activated alumina, J. Colloid Interface Sci. 333 (2009) 14–26.
[34] T.K. Naiya, A.K. Bhattacharya, S.K. Das, Adsorptive removal of Cd (II) ions from aqueous solutions by rice husk ash, Environ. Prog. 28 (2009) 535–546.
[35] T.K. Naiya, A.K. Bhattacharya, S.K. Das, Removal of Cd (II) from aqueous solutions using clarified sludge, J. Colloid Interface Sci. 325 (2008) 48–56.
[36] H. Koynucu, Adsorption kinetics of 3-hydroxybenzaldehyde on native and activated bentonite, Appl. Clay Sci. 38 (2008) 279–282.
[37] G. Mahajan, D. Sud, Application of ligno-cellulosic waste material for heavy metal ions removal from aqueous solution, J. Environ. Chem. Eng. (2013), http://dx.doi.org/10.1016/j.jece.2013.08.013.
[38] F. Ge, M.M. Li, H. Ye, B.X. Zhao, Effective removal of heavy metal ions Cd^{2+}, Zn^{2+}, Pb^{2+}, Cu^{2+} from aqueous solution by polymer-modified magnetic nanoparticles, J. Hazard. Mater. 211–212 (211) (2012) 366–370.
[39] Y. Ren, H.A. Abbood, F. He, H. Peng, K. Huang, Magnetic EDTA-modified chitosan/SiO_2/Fe_3O_4 adsorbent: preparation, characterization, and application in heavy metal adsorption, Chem. Eng. J. 226 (2013) 300–311.
[40] S. Cataldo, G. Cavallaro, A. Gianguzza, G. Lazzara, A. Pettignano, D. Piazzese, I. Villaescusa, Kinetic and equilibrium study for cadmium and copper removal from aqueous solutions by sorption onto mixed alginate/pectin gel beads, J. Environ. Chem. Eng. (2013), http://dx.doi.org/10.1016/j.jece.2013.09.012.
[41] J. Wang, B.L. Deng, X.R. Wang, J.Z. Zheng, Adsorption of aqueous Hg(II) by sulfur-impregnated activated carbon, Environ. Eng. Sci. 26 (2009) 1693–1699.
[42] E.I. El-Shafey, Removal of Zn(II) and Hg(II) from aqueous solution on a carbonaceous sorbent chemically prepared from rice husk, J. Hazard. Mater. 175 (2010) 319–327.
[43] D. Cyril, O.M. Fabrice, L. Bénédicte, W. Alain, J. Wan, Factors affecting the reactivity of thiol-functionalized mesoporous silica adsorbents toward mercury(II), Talanta 79 (2009) 877–886.
[44] S. Pan, Y. Zhang, H. Shen, M. Hua, An intensive study on the magnetic effect of mercapto-functionalized nano-magnetic Fe_3O_4 polymers and their adsorption mechanism for the removal of Hg(II) from aqueous solution, Chem. Eng. J. 210 (2012) 564–574.
[45] B.S. Inbaraj, J.S. Wang, J.F. Lu, F.Y. Siao, B.H. Chen, Adsorption of toxic mercury(II) by an extracellular biopolymer poly(c-glutamic acid), Bioresour. Technol. 100 (2009) 200–207.
[46] Y.S. Ho, C.C. Wang, Sorption equilibrium of mercury onto ground-up tree fern, J. Hazard. Mater. 156 (2008) 398–404.
[47] L. Zhou, Y.P. Wang, Z.R. Liu, Q.W. Huang, Characteristics of equilibrium, kinetics studies for adsorption of Hg(II), Cu(II), and Ni(II) ions by thiourea modified magnetic chitosan microspheres, J. Hazard. Mater. 161 (2009) 995–1002.
[48] R.J. Qu, Y. Zhang, C.M. Sun, C.H. Wang, C.N. Ji, H. Chen, P. Yin, Adsorption of Hg(II) from an aqueous solution by silica-gel supported diethylenetriamine prepared via different routes: kinetics, thermodynamics, and isotherms, J. Chem. Eng. Data 55 (2010) 1496–1504.
[49] F. Ma, R.J. Qu, C.M. Sun, C.H. Wang, C.N. Ji, Y. Zhang, P. Yin, Adsorption behaviors of Hg(II) on chitosan functionalized by amino-terminated hyperbranched polyamidoamine polymers, J. Hazard. Mater. 172 (2009) 792–801.
[50] G.X. Zong, Hou Chen, R.J. Qu, C.H. Wang, N.Y. Ji, Synthesis of polyacrylonitrile grafted cross-linked N-chlorosulfonamidated polystyrene via surface-initiated ARGET ATRP, and use of the resin in mercury removal after modification, J. Hazard. Mater. 186 (2011) 614–621.
[51] J. Chen, R.J. Qu, Y. Zhang, C.M. Sun, C.H. Wang, C.N. Ji, P. Yin, H. Chen, Y.Z. Niu, Preparation of silica gel supported amidoxime adsorbents for selective adsorption of Hg(II) from aqueous solution, Chem. Eng. J. 209 (2012) 235–244.
[52] R.J. Qu, M.H. Wang, R.F. Song, C.M. Sun, Y. Zhang, X.Y. Sun, C.N. Ji, C.H. Wang, P. Yin, Adsorption kinetics and isotherms of Ag(I) and Hg(II) onto silica gel with functional groups of hydroxyl- or amino-terminated polyamines, J. Chem. Eng. Data 56 (2011) 1982–1990.
[53] R. Qu, Y. Zhang, W. Qu, C. Sun, J. Chen, Y. Ping, H. Chen, Y. Niu, Mercury adsorption by sulfur- and amidoxime-containing bifunctional silica gel based hybrid materials, Chem. Eng. J. 219 (2013) 51–61.
[54] A.M. Donia, A.A. Atia, K.Z. Elwakeel, Selective separation of mercury(II) using magnetic chitosan resin modified with Schiff's base derived from thiourea and glutaraldehyde, J. Hazard. Mater. 151 (2008) 372–379.
[55] S. Pan, H. Shen, Q. Xu, J. Luo, M. Hu, Surface mercapto engineered magnetic Fe_3O_4 nanoadsorbent for the removal of mercury from aqueous solutions, J. Colloid Interface Sci. 365 (2012) 204–212.
[56] C.T. Kresge, M.E. Leonowicz, W.J. Roth, J.C. Vartuli, J.S. Beck, A new family of mesoporous molecular sieve prepared with liquid crystal templates, Nature 359 (1992) 710–719.
[57] J.Y. Ying, C.P. Mehnert, M.S. Wong, Synthesis and application of supramolecular-templated mesoporous materials, Angew. Chem. Int. Ed. 38 (1999) 56–77.
[58] M. Vallet-Regí, L. Ruiz-González, I. Izquierdo-Barba, J.M. González-Calbet, Revisiting silica based ordered mesoporous materials: medical applications, J. Chem. Mater. 16 (2006) 26–31.
[59] T. Witula, K. Holmberg, Use of different types of mesoporous materials as tools for organic synthesis, J. Colloid Interface Sci. 310 (2007) 536–545.
[60] C. Luengo, V. Puccia, M. Avena, Arsenate adsorption and desorption kinetics on Fe(III)-modified montmorillonite, J. Hazard. Mater. 86 (2009) 1713–1719.
[61] S. Mason, C. Iceman, K. Tanwar, T. Trainor, A. Chaka, Pb(II) adsorption on isostructural hydrated alumina and haematite (0 0 0 1) surfaces: a DFT study, J. Phys. Chem. C 113 (2011) 2159–2170.
[62] A. Prado, L. Arakaki, C. Airoldi, Adsorption and separation of cations on silica gel chemically modified by homogeneous and heterogeneous routes with the ethyleneimine anchored on thiol modified silica gel, Green Chem. 4 (2002) 42–46.
[63] W.S. Hummers, R.E. Offeman, Preparation of graphitic oxide, J. Am. Chem. Soc. 80 (6) (1958) 1339.
[64] Y.S. Ho, J.C.Y. Ng, G. Mckay, Kinetics of pollutant sorption by biosorbents: review, Sep. Purif. Methods 29 (2000) 186–232.
[65] Y.S. Ho, G. McKay, Pseudo-second order model for sorption processes, Process Biochem. 34 (5) (1999) 451–465.
[66] S. Lagergren, Zur theorie der sogenannten adsorption geloster stoffe, Kungliga SVenska Vetenskapsakademiens, Handlingar Band. 24 (1898) 1–39.
[67] K. Aparecida, G. Gusmao, L.V.A. Gurgel, T.M.S. Melo, F. Gil, Application of succinylated sugarcane bagasse as biosorbent to remove methylene blue and gentian

violet from aqueous solutions—kinetic and equilibrium studies, Dyes Pigm. 92 (2012) 967–974.
[68] Y.P. Xu, F.W. Schwartz, S.J. Traina, Sorption of Zn^{2+} and Cd^{2+} on hydroxyapatite surfaces, Environ. Sci. Technol. 28 (1994) 1472–1480.
[69] X. Yang, B. Al-Duri, Kinetic modeling of liquid-phase adsorption of reactive dyes on activated carbon, J. Colloid Interface Sci. 287 (2005) 25–34.
[70] W.J. Weber Jr., J.C. Morris, Kinetics of adsorption on carbon from solution, J. Sanit. Eng. ASCE 89 (1963) 31–59.
[71] F.-C. Wua, R.-L. Tseng, R.-S. Juang, Characteristics of Elovich equation used for the analysis of adsorption kinetics in dye-chitosan systems, Chem. Eng. J. 150 (2009) 366–373.
[72] F.A. Pavan, E.C. Lima, S.L.P. Dias, A.C. Mazzocato, Methylene blue biosorption from aqueous solutions by yellow passion fruit waste, J. Hazard. Mater. 150 (2008) 703–712.
[73] P.R. Wright, F.M. Muzzio, B.J. Glasser, Batch uptake of lysozyme: effect of solution viscosity and mass transfer on adsorption, Biotechnol. Prog. 56 (1998) 3149–3162.
[74] F.A. Shehata, M.F. Attallah, E.H. Borai, M.A. Hilal, M.M. Abo-Aly, Sorption reaction mechanism of some hazardous radionuclides from mixed waste by impreganated crown ether onto polymeric resin, Appl. Radiat. Isotopes 68 (2010) 239–249.
[75] T. Vermeulen, G. Klein, N.K. Hiester, Adsorption and Ion Exchange, McGraw-Hill, New York, USA, 1973.
[76] P. Zarabadi-Poor, A. Badiei, B.D. Fahlman, P. Arab, G.M. Ziarani, One-pot synthesis of ethanolamine-modified mesoporous silica, Ind. Eng. Chem. Res. 50 (2011) 10036–10040.
[77] L. Sun, H. Yu, B. Fugetsu, Graphene oxide adsorption enhanced by in situ reduction with sodium hydrosulfite to remove acridine orange from aqueous solution, J. Hazard. Mater. 203–204 (2012) 101–110.
[78] E.I. Unuabonah, K.O. Adebowale, B.I. Olu-Owolabi, L.Z. Yang, Comparison of sorption of Pb^{2+} and Cd^{2+} on Kaolinite clay and polyvinyl alcohol-modified Kaolinite clay, Adsorption 14 (2008) 791–803.
[79] I. Mobasherpour, E. Salahi, M. Pazouki, Comparative of the removal of Pb^{2+}, Cd^{2+} and Ni^{2+} by nanocrystallite hydroxyapatite from aqueous solutions: adsorption isotherm study, Arabian J. Chem. 5 (2012) 439–446.
[80] www.science.uwaterloo.ca/∼cchieh/cact/applychem/hydration.html, enthalpy of hydration, 4 April, 2013.
[81] S. Wang, H. Sun, H.M. Ang, M.O. Tadé, Adsorptive remediation of environmental pollutants using novel graphene-based nanomaterials, Chem. Eng. J. 226 (2013) 336–347.
[82] A.A. Alhwaige, T. Agag, H. Ishidab, S. Qutubuddin, Biobased chitosan hybrid aerogels with superior adsorption: role of graphene oxide in CO_2 capture, RSC Adv. 3 (2013) 16011–16020.